Estuaries and Coasts (2010) 33:1420–1429
DOI 10.1007/s12237-010-9313-2

Satellite Estimates of Wide-Range Suspended Sediment Concentrations in Changjiang (Yangtze) Estuary Using MERIS Data

Fang Shen · Wouter Verhoef · Yunxuan Zhou · Mhd. Suhyb Salama · Xiaoli Liu

Received: 18 August 2009 / Revised: 3 June 2010 / Accepted: 4 June 2010 / Published online: 22 June 2010

Abstract The Changjiang (Yangtze) estuarine and coastal waters are characterized by suspended sediments over a wide range of concentrations from 20 to 2,500 mg l^{-1}. Suspended sediment plays important roles in the estuarine and coastal system and environment. Previous algorithms for satellite estimates of suspended sediment concentration (SSC) showed a great limitation in that only low to moderate concentrations (up to 50 mg l^{-1}) could be reliably estimated. In this study, we developed a semi-empirical radiative transfer (SERT) model with physically based empirical coefficients to estimate SSC from MERIS data over turbid waters with a much wider range of SSC. The model was based on the Kubelka–Munk two-stream approximation of radiative transfer theory and calibrated using datasets from in situ measurements and outdoor controlled tank experiments. The results show that the sensitivity and saturation level of remote-sensing reflectance to SSC are dependent on wavelengths and SSC levels. Therefore, the SERT model, coupled with a multi-conditional algorithm scheme adapted to satellite retrieval of wide-range SSC, was proposed. Results suggest that this method is more effective and accurate in the estimation of SSC over turbid waters.

F. Shen (✉) · Y. Zhou · X. Liu
State Key laboratory of Estuarine and Coastal Research,
East China Normal University,
Shanghai 200062, China
e-mail: fshen@sklec.ecnu.edu.cn

W. Verhoef (✉) · M. S. Salama
Faculty of Geo-information Science and Earth Observation ITC,
University of Twente,
P.O. Box 6, 7500AA Enschede, The Netherlands
e-mail: verhoef@itc.nl

Keywords MERIS data · Semi-empirical radiative transfer model · Suspended sediment concentration · Turbid waters · Changjiang estuary

Introduction

Suspended sediment concentration (SSC) can directly influence the turbidity and color of water bodies (Miller and McKee 2004; Hu et al. 2004). The temporal–spatial distribution of SSC in estuarine and coastal waters is quite complicated and strongly affected by the variations of seasonal riverine discharges, tidal currents, and wind-driven resuspensions of the bottom sediments (Chen et al. 2003; Krivtsov et al. 2009). Better understanding of SSC distribution is critical for the analysis of geomorphologic evolutions, rates of erosion and sedimentation, riverine fluxes, and aquatic environments.

Ocean color observation from space can provide nearly daily synoptic views of the distribution of water substances and concentrations over large spatial and temporal coverages, which is not available from other sources. Global distribution of chlorophyll concentrations over case 1 oceanic waters can be estimated directly from ocean color products (Lee and Hu 2006; Dasgupta et al. 2009). In recent years, there is an increasing interest in satellite retrievals of water substances and concentrations for optically complex case 2 coastal waters. However, in the Changjiang estuary and coast, the standard ocean color products like Sea-Viewing Wide Field-of-View Sensor (SeaWiFS) and the Moderate Resolution Imaging Spectroradiometer (MODIS) products always exhibit "invalid data" labeled on the resultant SSC mappings. This is mainly due to the fact that the algorithms of SSC retrieval were not appropriate for the case 2 waters (IOCCG 2000). The SSC values from the MEdium Resolution

Imaging Spectrometer (MERIS) level 2 products partially display invalid flags raised over the Turbid Maximum Zone (TMZ) of our study area, which are improved a bit by the MERIS Case 2 waters Regional (C2R) processor (Doerffer and Schiller 2008), but basically underestimated. This may be attributed to the presently available neural networks in the C2R processor for atmospheric correction and the SSC retrieval (Doerffer and Schiller 2007) not being trained for the high SSC of the Changjiang estuary and coast and these areas being out of scope of the C2R.

For satellite estimates of high SSC, empirical algorithms, such as the algorithms of ratio of the MODIS red band to near-infrared (NIR) band developed by Doxaran et al. (2002, 2009) and of the single MODIS red band adopted by Miller and McKee (2004), were established. They could be adapted for narrow-range high SSC and would introduce larger errors for low SSC. Semi-analytical algorithms analyzing the relationships among R_{rs}, absorption, and backscattering coefficients related to SSC (Fettweis et al. 2007; Hu et al. 2004) were mainly applied to low or moderate SSC waters.

Facing those situations, it is urgent to develop new SSC retrieval algorithms adapted for turbid waters with a wide-range SSC, which indeed exists in the Changjiang estuary and coast. In these areas, the surface SSC values range from 100 to 300 mg l^{-1} in the South Branch, from 300 to 500 mg l^{-1} in the TMZ (e.g., in the South and North Passages and North Harbor), above 500 mg l^{-1} in the Hangzhou Bay, and below 50 mg l^{-1} off the turbidity front seawards. These values were roughly acknowledged by investigators in recent years (Chen et al. 2003; Kong et al. 2006). However, such wide-range SSC has not been involved in currently available algorithms of satellite retrieval so far. The purpose of the present study was to develop an algorithm for accurately estimating SSC over turbid waters with a wide range from low SSC (below 20 mg l^{-1}) to high or super-high SSC (above 250 mg l^{-1}) using MERIS data. A semi-empirical radiative transfer (SERT) model based on the Kubelka–Munk two-stream approximation of radiative transfer theory, coupled with a multi-conditional algorithm scheme for the wide-range SSC, is to be explored.

Materials

Study Area

The Changjiang (Yangtze River) estuary is located on the east coast of China and close to the East China Sea (See Fig. 1). From 1951 to 2000, the Changjiang River has discharged an annual average of about 9×10^{11} m^3 of water and 4×10^8 tons of sediment into its estuary (Chen et al. 2003). The dispersal of the Changjiang influx into the East China Sea forms turbid plumes extending eastward over an area of 10^4–10^5 km^2 in the summer (Zhang et al. 2007). The sediment discharges are strongly affected by the dry and flood season variations (Chen et al. 2003). About 87% of the annual total sediment discharges in the flood season (i.e., from June to September). About 50% of the sediments carried by the Changjiang River are accumulated at the river mouth, forming large submerged deltas and mouth bars (Shen and Pan 2001). The SSC values span two orders of magnitude and range from 20 mg l^{-1} (e.g., off the river mouth) to 2,500 mg l^{-1} or even more (e.g., in the TMZ; Li et al. 1994) in the Changjiang Estuary. Based on investigations for the SSC distribution, including the SSC from surface to bottom (in fact, surface SSC lower than bottom SSC), He et al. (1999) concluded that the Changjiang estuarine water was roughly divided into four regions of SSC levels: (1) the super-highly turbid water, located 121°55′ E–122°15′ E, with an average between 500 and 900 mg l^{-1} and a maximum value up to 2,500 mg l^{-1} in the South Passage; (2) the highly turbid water, located at 122°15′ E–122°30′ E, with an average between 250 and 500 mg l^{-1}; (3) moderately turbid waters, which correspond to a shallow sea region with water depth of 15–30 m (>122°30′ E), with an average between 80 and 250 mg l^{-1}; and (4) low turbid waters, e.g., located beyond 30-m water depth, with the SSC level below 80 mg l^{-1}. The SSC magnitudes and distributions in the four regions were changed slightly due to the decreased sediment discharges in recent years (Yang et al. 2007).

In Situ Datasets

In situ datasets were collected from mooring observations during dry and flood seasons of 2003–2007 and cruise surveys during April and August of 2008, respectively. Numbers of boat-mooring stations were concurrently and symmetrically distributed over the Changjiang estuary where samplings were simultaneously taken at 1-h interval. The cruise surveys covered the Changjiang estuary and its adjacent East China Sea. Radiometric measurements were conditionally taken during the campaigns of September 2004, July and August 2005, February 2006, and April and August 2008, limited by instrument availability. The number of valid measurements was also confined by weather conditions, i.e., wind speed and cloud cover. The SSC samplings and radiometric measurements were conducted simultaneously, as data matchups, for use in the calibrations of the SERT model. Other in situ SSC were used for the validation of the model.

Practically, it is difficult to capture the variations of SSC gradients from low to high levels and the simultaneous radiometric measurements taken under the conditions of sunlight, cloud-free, and moderate wind speed during the campaigns. In addition, in situ datasets are often geographically and seasonally biased due to constraints in the timing and location of oceanic cruises (Claustre and Maritorena

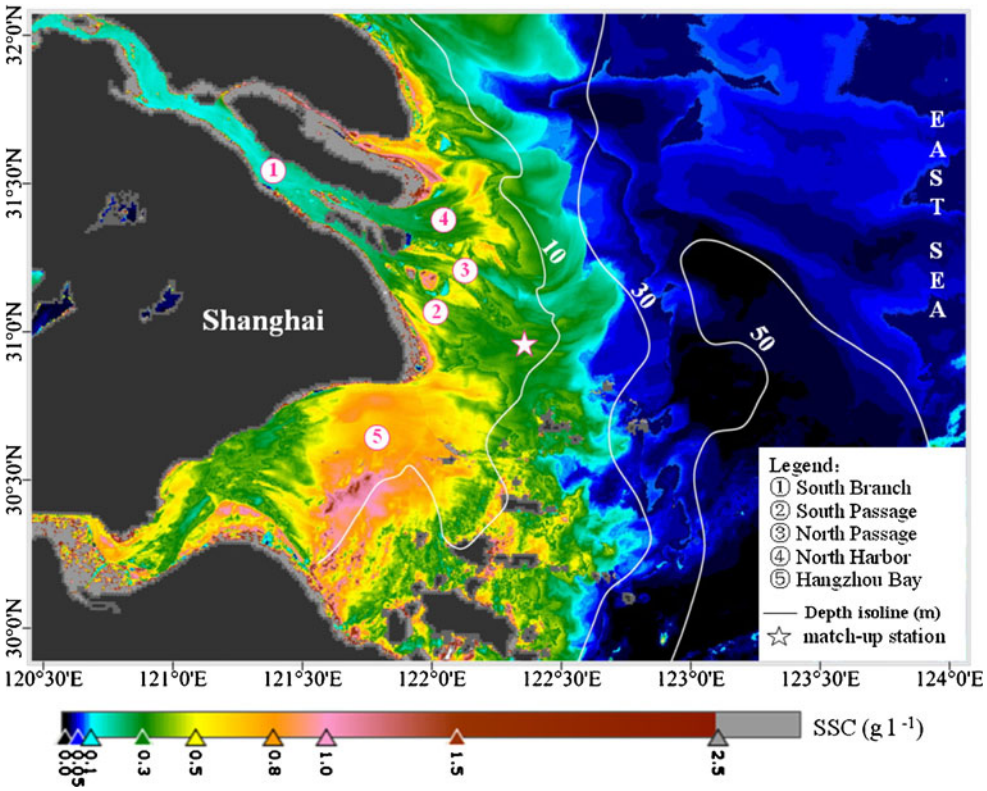

Fig. 1 Mapping of suspended sediment concentration (*SSC*) retrieved from the MERIS data of April 25, 2008 over the Changjiang estuary and coast

2003). Therefore, as complementary to samplings and in situ measurements, controlled outdoor tank experiments were conducted during July 2006.

The tank experiments were taken outdoors in a black experimentation tank (height, 1.5 m; diameter of cylinder top, 1.5 m; diameter of cylinder bottom, 1.4 m). Sediment samples each with 25 g in weight were gradually put into the tank once per 10 min to increase concentration, churned up to be approximately distributed homogenous in the water column with a turbidity meter for surveillance, and afterwards carried out above-water radiometric measurements and water samplings (more details in Shen et al. 2010). Most particles of sediment samples with mean grain sizes ranging between 7 and 40 μm would not have sufficient time to settle in short moments of the radiometric measurements by actual observations. The sediment samples of the tank experiments were originated from tidal flats of Yangtze River and Yellow River estuaries, respectively, for the investigation of whether sediment material types of two typical estuaries in China Coast would significantly affect the remote-sensing reflectance. The result exhibited a weak effect of the different sediment materials on reflectance. This is meaningful for algorithms to be possibly applied to other places.

In this study, in situ SSC data were based on surface water samplings. The concentrations were determined gravimetrically by filtering the water samples on 0.7-μm Whatman GF/F glass fiber filters. All filters were rinsed with Milli-Q water to remove salts, dried, and then reweighed on a high-precision balance in the laboratory.

Radiometric measurements were recorded with the ASD Fieldspec Pro spectroradiometer (ASD Inc.) covering the wavelength range from 350 to 2500 nm (at 1.4 nm sampling intervals in the 350–1,000 nm spectral domain and at 2 nm intervals in the range of 1,000–2,500 nm). The procedure for above-surface radiometric measurements for determining remote-sensing reflectance (R_{rs}) can be referred to Lee et al. (1996) and Mobley (1999) for details. The observation geometry is a crucial part of the above-surface measurement. The radiance sensor must point to sea and sky at the same nadir and zenith angles. These angles are usually chosen to be between 30° and 50° with an optimum angle of 40°, as recommended in the SeaWiFS protocol (Fargion and Muller 2000). At this angle, the sea surface reflectance for the skylight does not depend greatly on the wind speed. To avoid the direct sun glint, the sensor should be pointed at the azimuth angle between 90° and 180° away from solar plane, with an optimum angle of 135° away from sun. With this orientation, the glint effect will be minimized and water-leaving radiance will dominate the total signal.

MERIS Data

MERIS as one of Envisat satellite payloads was launched by the European Space Agency (ESA) in 2002. Its configurations were listed in Table 1 where sun irradiance

Table 1 MERIS sensor configurations

Band no.	Band center (nm)	Bandwidth (nm)	Solar irradiance[a] ($Wm^{-2}nm^{-1}$)
1	412.5	10	1,713.642
2	442.5	10	1,877.436
3	490	10	1,929.326
4	510	10	1,926.839
5	560	10	1,800.486
6	620	10	1,649.71
7	665	10	1,530.904
8	681.25	7.5	1,470.226
9	708.75	10	1,405.469
10	753.75	7.5	1,266.199
11	761.875	2.5	1,249.882
12	778.75	15	1,175.723
13	865	20	958.8855
14	885	10	929.7632
15	900	10	895.4086

Field of view: 68.5° centered about nadir; swath width: 1150 km

Spatial resolution: RR (1,040×1,200 m), FR (260×300 m)

Radiometric accuracy: <2% in reflectance (relative to the sun irradiance)

Signal-to-noise ratio: 1,650 (at 412.5 nm) for typical ocean signal

[a] The solar irradiance (not day-corrected) are integrated over the spectral widths of the band

data were from http://www.brockmann-consult.de/beam/doc/help/smile/SmileCorrAlgorithmSpecification.html and others from Bézy et al. (2002). Currently released products for users involve the MERIS level 1b, including radiances at top-of-the-atmosphere (TOA) and ancillary data and the MERIS level 2, including retrieved remote-sensing reflectance (also termed water-leaving radiance reflectance), ocean color products including SSC, chlorophyll concentration, etc., as well as atmospheric parameters and ancillary data. In this study, the MERIS 1b TOA radiances were used for the retrieval of the remote-sensing reflectance, R_{rs}, by our atmospheric correction approach since the MERIS level 2 R_{rs} data over the turbid waters were underestimated by investigation of this study (see "Performance of Atmospheric Correction for MERIS Level 1b Data"). As an evidence, the MERIS level 2 R_{rs} data were employed for the comparison with in situ R_{rs}.

Methodology

Atmospheric Correction

Atmospheric correction is one of the most limiting factors for accurate retrieval of water constituents from satellite data in turbid waters (Schroeder et al. 2007). Ocean color standard algorithms of atmospheric correction for satellite imagery are based on the assumption of zero water-leaving radiance in the NIR spectral region (Gordon and Wang 1994). These algorithms are more appropriate for case 1 waters, and the assumption would lead to the underestimation of water-leaving radiances in turbid waters (IOCCG 2000). For atmospheric correction of case 2 coastal waters, an algorithm based on inverse modeling of radiative transfer calculations using artificial neural network techniques was developed for the processing of MERIS level 1b data (Schroeder et al. 2007). However, the resultant MERIS level 2 R_{rs} data were still underestimated when compared with in situ R_{rs} (see "Performance of Atmospheric Correction for MERIS Level 1b Data"). This could to be attributed to exceptional cases like those occurring in the Changjiang estuary. Developing an algorithm of atmospheric correction over the turbid waters is out of scope of this study. Instead, an atmospheric radiative transfer (RT) model was employed for creating the lookup tables (LUTs) simulated by various atmospheric conditions and viewing geometries. The modeling of atmospheric effects based on RT equations is detailed in Appendix 1. Through the LUTs, surface remote-sensing reflectance leaving the waters can be inverted from the MERIS level 1b TOA radiances.

SERT Model

Remote-sensing reflectance (R_{rs}) is simply expressed as follows (Carder et al. 1993; Mobley 1999):

$$R_{rs} = \frac{L_w}{E_d},$$

where E_d is the downwelling irradiance just above the sea surface and L_w is the directional water-leaving radiance. They are wavelength-dependent.

Remote-sensing reflectance is related to inherent optical properties of the water through the underwater irradiance reflectance. Underwater reflectance of an optically deep (semi-infinite) turbid medium is given by (Kubelka and Munk 1931):

$$r_\infty = \frac{b_b}{b_b + a + \sqrt{(b_b + a)^2 - {b_b}^2}}, \quad (1)$$

where b_b is the backscatter coefficient and a is the absorption coefficient. From Eq. 1, the infinite reflectance can also be calculated by:

$$r_\infty = \frac{\frac{b_b}{a}}{1 + \frac{b_b}{a} + \sqrt{1 + 2\frac{b_b}{a}}}. \quad (2)$$

Equation 2 shows that the infinite reflectance is only a function of the *ratio* of backscattering and absorption. If

this ratio is small, such as for most waters, one can approximate the infinite reflectance by:

$$r_\infty = \frac{\frac{b_b}{a}}{2\left(1+\frac{b_b}{a}\right)} = 0.5\frac{b_b}{a+b_b}, \quad (3)$$

which is similar to the result of many optical water models since these are often functions of the ratio $b_b/(a+b_b)$ (e.g., Gordon et al. 1975).

Suspended sediment matter in water mainly has an impact on the scattering and not so much on the absorption. Therefore, a semi-empirical model can be constructed for water containing the sediment, which is based on two unknown constants α and β. This model displays a behavior similar to Eq. 2. It predicts the remote-sensing reflectance, R_{rs}, by:

$$R_{rs} = \frac{\alpha\beta C_{ss}}{1+\beta C_{ss}+\sqrt{1+2\beta C_{ss}}}, \quad (4)$$

where C_{ss} stands for the SSC in arbitrary units. The constants α and β have simple but meaningful interpretations. The constant α is equal to the theoretical R_{rs} at infinite C_{ss}, so it represents the saturation level of the reflectance; $4/\beta$ represents the SSC for $R_{rs}=1/2\alpha$ in the SERT model. This is also approximately the point of maximum sensitivity (on a log scale for SSC).

The SERT model is simple and operational and has the advantages of: (1) physically meaningful parameters; (2) R_{rs} values of the forward model stay within physically possible bounds, as a function of SSC for concentrations from zero to infinity; and (3) application in sensitivity analysis (discussed in "Sensitivity Analysis").

Results and Discussion

Performance of Atmospheric Correction for MERIS Level 1b Data

Atmospheric correction was performed to the MERIS level 1b TOA radiances data using the aforementioned method. In this study, the Ge Lake (31.6° N/119.81° E, 146.5 km^2 in area) or offshore seawaters was selected as a known dark target, and the mouth bar in the TMZ as a known bright target, in order to find the best match between measured R_{rs} and modeled R_{rs} spectra with the aid of the LUTs.

Very limited number of MERIS scenes instantaneously overpassing the Changjiang estuary was matched up with simultaneously in situ measured R_{rs} data. The R_{rs} matchups were used for the validation of the inverted R_{rs} from MERIS level 1b TOA radiances via our atmospheric correction approach. A comparison of the inverted R_{rs} by our approach, MERIS level 2 R_{rs} data and coincident in situ R_{rs} measured at one station (shown in Fig. 1, as an example) located in the turbid waters, is illustrated in Fig. 2. The in situ R_{rs} was measured at 9:30 A.M. (local time) on 4 August 2008, with coincident MERIS overpass at 10:00 A.M. of the same day. Overcorrection of the atmospheric path reflectance in MERIS level 2 R_{rs} data was noticed so that the MERIS level 2 R_{rs} data were underestimated in the whole MERIS bands. The inverted R_{rs} showed a better agreement with in situ R_{rs} in the red through NIR bands and a little underestimation in the green bands and basically yielded acceptable results except in the blue bands.

Although the atmospheric correction of MERIS level 1b data based on the LUTs gave a substantial improvement of inverted R_{rs} over the turbid waters, the limitation of the method is that adjacency effects (i.e., pixels close to land) and the assumption of a homogeneous sea surface would introduce errors in this inversion. It is expected that these errors are moderate compared to the errors related to heterogeneities (spatially variable haze) in the atmosphere. An alternative method which takes into account this spatially variable haze conditions will be proposed in Shen and Verhoef (2010).

Application of the SERT Model for SSC Retrieval

Determination of the SERT Parameters

Simultaneously measured R_{rs} and SSC data matchups from in situ measurements (36 samples) and tank-based measurements (82 samples) were available for the determination of fitting parameters α and β of the SERT model according to Eq. 4 through the procedure of nonlinear iterative regression. The two parameters were wavelength-dependent and listed in Table 2. The fitting curve, given by the regression between the measured R_{rs} at 778 nm and the logarithmic SSC as an example, is shown

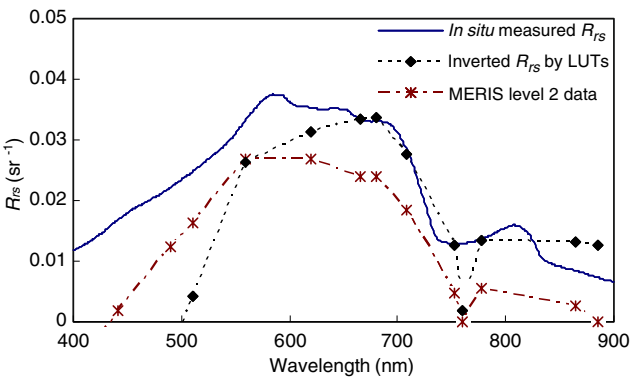

Fig. 2 In situ R_{rs} spectrum (*solid line*) and inverted R_{rs} spectrum (*dotted line*) from MERIS 1b TOA radiances by our atmospheric correction approach and the standard MERIS level 2 R_{rs} spectrum (*dotted + dashed line*). The in situ R_{rs} was measured at 9:30 A.M. (local time) on 4 August 2008, with coincident MERIS overpass at 10:00 A.M. of the same day

Table 2 Two parameters of the SERT model at candidate MERIS bands

MERIS bands (nm)	α	β	Correlation (r^2, n=118)
412	0.0201	49.6982	0.465
442	0.0252	48.4005	0.464
490	0.0311	47.5101	0.467
510	0.0347	45.0726	0.465
560	0.0493	35.3352	0.482
620	0.0652	20.4711	0.558
709	0.076	10.61	0.640
779	0.0904	3.5027	0.752

They are predicted by the nonlinear iterative regression of measured R_{rs} and SSC data matchups (36 samples from in situ measurements, 82 samples from tank experiments)

in Fig. 3. All the R_{rs} spectral data predicted by the SERT model corresponding to the MERIS bands are shown in Fig. 4.

In this present study, the SERT model parameters were dependent on in situ datasets. It is expected that they would be linked to backscattering and absorption coefficients of suspended sediment matters in turbid waters in our future work.

Sensitivity Analysis

The sensitivity of R_{rs} to relative changes in SSC was estimated for the MERIS bands and illustrated in Fig. 5. The sensitivity of R_{rs} to SSC is not only wavelength-dependent but also SSC level-dependent. The R_{rs} at shorter wavebands is more sensitive to low SSC and that at longer wavebands to high SSC. According to the sensitivity analysis, one can find the most sensitive bands for various ranges of SSC: the MERIS band 560 nm for log (SSC) < −1.7 in unit of grams per liter; the band 620 nm for −1.7 > log (SSC) > −1.1 in unit of grams per liter; the band 708 nm for −1.1 > log (SSC) > −0.6 in unit of grams per liter; and the band 778 nm for log (SSC) > −0.6 in unit of grams per liter. This implies that wide-range SSC retrievals from R_{rs} should be based on R_{rs} multispectral data.

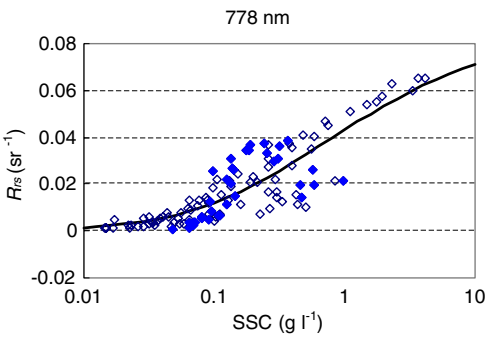

Fig. 3 Regression curve based on the SERT model of measured R_{rs} at MERIS band 778 nm against SSC data from in situ measurements (*solid diamonds*) and tank experiments (*empty diamonds*)

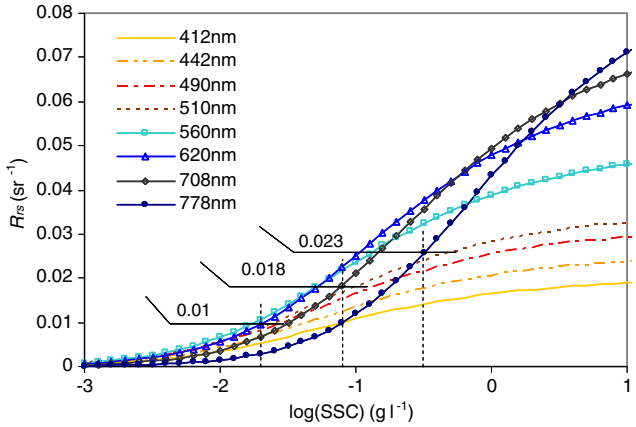

Fig. 4 Predicted R_{rs} by the SERT model for candidate MERIS bands, with various SSC levels

Multi-conditional Algorithm Scheme

As discussed above, various levels of SSC should be derived from the corresponding most sensitive R_{rs} spectra. In Fig. 4, one can find the corresponding R_{rs} levels. These are: R_{rs} (620) = 0.01 at log (SSC) = −1.7; R_{rs} (708) = 0.018 at log (SSC) = −1.1; and R_{rs} (778) = 0.023 at log (SSC) = −0.6 (i.e., at the intersections). These resemble the thresholds of R_{rs} spectra sensitive to SSC variations.

Therefore, the scheme for SSC retrieval from the R_{rs} multispectral data is given by multiple conditional expressions like:

If $R_{rs}(620) < 0.01$ Then
  use R_{rs} data at 560 nm for SSC retrieval by the SERT model
Else If $R_{rs}(708) < 0.018$ Then
  use R_{rs} data at 620 nm
Else If $R_{rs}(778) < 0.023$ Then
  use R_{rs} data at 708 nm
Else
  use R_{rs} data at 778 nm
End If.

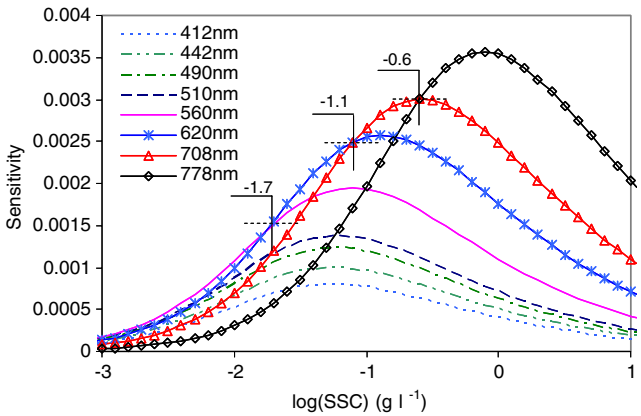

Fig. 5 Sensitivity of R_{rs} to relative changes in SSC for MERIS bands

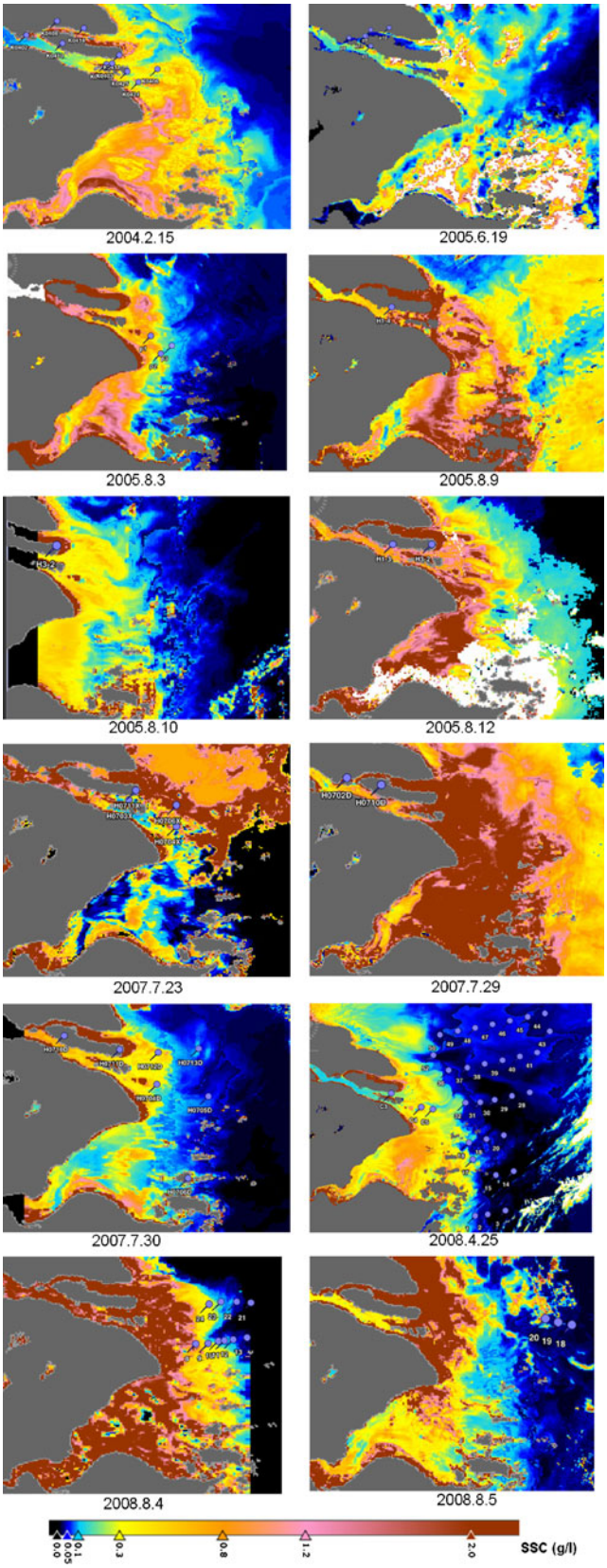

Fig. 6 Retrieved SSC mappings using the SERT model coupled with the multi-conditional algorithm scheme from atmospherically corrected R_{rs}. The R_{rs} was inverted by our atmospheric correction approach from MERIS level 1b TOA radiance data. *Pinpoints* on the mappings denote coincident in situ SSC samplings with MERIS overpasses

The algorithm scheme based on variable bands for wide-range SSC retrieval from the R_{rs} multispectral data is better able to avoid situations of R_{rs} saturation or of decline of R_{rs} sensitivity at certain wavelengths so as to reduce large errors in SSC estimates. As a result, we proposed to use 560 nm for low SSC (below 20 mg l^{-1}), 620 nm for moderate SSC (20–80 mg l^{-1}), 708 nm for high SSC (80–250 mg l^{-1}), and 778 nm for super-high SSC (above 250 mg l^{-1}).

MERIS Retrieval of SSC

The performance of the SERT model coupled with the multi-conditional algorithm scheme was thereafter conducted for the inverted R_{rs} from MERIS level 1b TOA radiances by our atmospheric correction procedure to retrieve SSC.

It was found in Fig. 1 that the retrieved SSC from the MERIS level 1b image of 25 April 2008, as an example of performance of those methods, in magnitude and spatial distribution, exhibited a better match with field observations. The SSC in the TMZ ranged from 300 to 700 mg l^{-1}, increased to 800 mg l^{-1} or more in the Hangzhou Bay, and declined to <100 mg l^{-1} off the turbidity front seawards. Since the clear waters (e.g., SSC < 20 mg l^{-1}) stay near the coast with a depth above 40 m, the bottom effects for the surface remote-sensing reflectance leaving the waters can be neglected for this case. The remote-sensing reflectance of turbid waters regarded as optically infinite deep waters are generally assumed to be unaffected by the bottom reflectance.

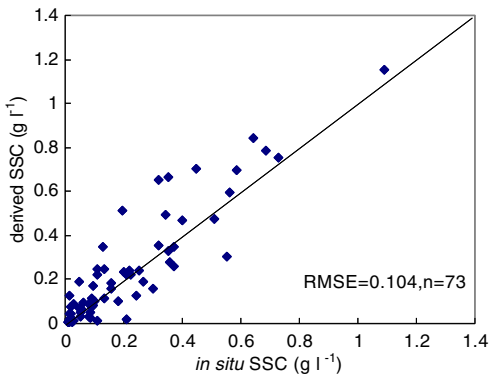

Fig. 7 Comparison of in situ SSC and retrieved SSC by the SERT model coupled with the multi-conditional algorithm scheme. In situ SSC data were concurrently measured at the moment of MERIS overpass the study area

Comparison of Retrieved and Measured SSC

Twelve MERIS scenes from 15 February of 2004; 19 June and 3, 9, 10, 12 August of 2005; 23, 29, 30 July of 2007; and 25 April and 4, 5 August of 2008 were available and coincident with 44 samples of in situ SSC collected within ±1 h offset of the moment of MERIS overpass and 29 samples (mostly off the mouth seawards, SSC < 50 mg l^{-1}) within the same cruise survey of April 2008. The coincident matchups were used for the validation of the SSC retrieval algorithm. The resulting SSC mappings from the MERIS level 1b images by the performance of our methods with the coincident in situ SSC samplings at 73 pinpoints are displayed in Fig. 6 where the deep red-colored pixels in the images of August 9 in 2005; July 23, 29 in 2007; and August 4, 5 in 2008 are most likely suspicious, mainly due to the contaminations of patchy haze.

A comparison of the retrieved SSC to the in situ SSC data is illustrated in Fig. 7. The root mean square error (RMSE) of both was statistically calculated, i.e., RMSE = 0.104 gl^{-1}, n=73 (samples). In fact, among the data matchups, the RMSE of 63 samples was 0.055 gl^{-1}, and the other ten samples introduced larger errors.

The biases of the matchups would be attributed to the high variability of sediment dynamics in the Changjiang estuary. Such high variability of SSC temporal–spatial distribution in the estuary and coast make it unlikely that in situ samplings would always agree with satellite instantaneous overpass. In addition, the precision of SSC retrieval is relevant to the remote-sensing reflectance which depends on the accuracy of atmospheric correction of satellite data.

Conclusion

Reliable methods to estimate aquatic biogeophysical parameters in the case 2 waters are in urgent need. In this paper, we employed the LUTs simulated by an atmospheric radiative transfer model to invert R_{rs} from MERIS 1b TOA radiances data over turbid waters. We developed a new formulation to quantify suspended sediment concentration, which was based on a SERT model with physically based empirical coefficients. We proposed the SERT model coupled with a multi-conditional algorithm scheme to derive SSC from the inverted R_{rs} multispectral data for turbid waters with a wide range of SSC. This method was then validated with in situ measurements using MERIS–in situ data matchups. The following conclusions are drawn from the presented analysis in this work:

1. The proposed model of SSC retrieval is physically based. The two empirical coefficients of the model can be associated with the sensitivities and saturation levels of R_{rs}, as well as the corresponding SSC for MERIS bands.
2. The proposed multi-conditional algorithm scheme can be adapted for the retrieval of SSC with a wide range. According to this study, 560 nm for low SSC (below 20 mg l^{-1}), 620 nm for moderate SSC (20–80 mg l^{-1}), 708 nm for high SSC (80–250 mg l^{-1}), and 778 nm for super-high SSC (above 250 mg l^{-1}) are optimal for concentration estimations. Of course, SSC ranges can be tuned with respect to the regional situations of the sensitivities and saturation levels of R_{rs}.
3. Results of our method are considerably more accurate than the standard MERIS level 2 products, at least in the studied areas.
4. The developed model of SSC retrieval is generic and can be applied to different regions with known typical SSC levels. The empirical coefficients in the SERT model can be derived from regional measurements.

Acknowledgments This research was funded by National Natural Science Foundation of China (no. 40871165) and the "111 Project" (B08022). Field data were supported by the Creative Research Groups of China from the NSFC (no. 40721004) and the "973 National Basic Research Program." The authors are grateful to scientists and graduate students from our laboratory for their assistance in in situ measurements and samplings. Thanks to the European Space Agency (ESA) for providing MERIS data via the support of ESA approved Cat-1 project (id. 4359). We are grateful to three anonymous reviewers and editors for their helpful comments and suggestions.

Appendix 1. Atmospheric Correction Based on the Radiative Transfer Model

For a hypothetical homogeneous Lambertian sea surface with the surface reflectance r, the total radiance at the top of the atmosphere (TOA) can be calculated according to the following equation (Verhoef and Bach 2003):

$$L^{\mathrm{TOA}} = \frac{E_s^0 \cos\theta_s}{\pi}\left[\rho_{so} + \frac{(\tau_{ss}+\tau_{sd})r(\tau_{do}+\tau_{oo})}{1-r\rho_{dd}}\right]. \quad (1)$$

Here, the ρ and τ symbols with double subscripts are intrinsic optical properties (reflectances and transmittances) of the entire atmosphere layer. The subscripts indicate the respective kinds of incident and exiting radiation, namely s for direct solar flux, d for upward or downward diffuse

flux, and o for radiance in the observer's direction. Furthermore, $E_s^0$is the extraterrestrial solar irradiance (corrected for sun–earth distance), and θ_s is the solar zenith angle. Without any loss of generality, one can simplify the above equation to:

$$L^{\mathrm{TOA}} = L_0 + \frac{Gr}{1 - rS} \tag{2}$$

where $L_0 = \rho_{so} \frac{E_s^0 \cos\theta_s}{\pi}$ is the atmospheric path radiance for zero surface reflectance; $S = \rho_{\mathrm{dd}}$ is the so-called spherical albedo or the bi-hemispherical reflectance of the bottom of the atmosphere, and G is a gain factor, i.e., $G = \frac{E_s^0 \cos\theta_s}{\pi}(\tau_{ss} + \tau_{sd})(\tau_{do} + \tau_{oo})$, which contains the product of total downward and upward transmittance. Equation 2 is nonlinear in r, but since sea surface reflectance r and the spherical albedo S are mostly quite small, the nonlinearity remains very limited. Note that adjacency effects are ignored here.

The parameters L_0, S, and G can be estimated from the outputs of an atmospheric RT model like MODTRAN (Berk et al. 2000) by running the model for surface reflectances of 0.0, 0.5, and 1.0, respectively. The MODTRAN total TOA radiance outputs for surface reflectances of 0.0, 0.5, and 1.0 are named LTOT_0, LTOT_{50}, and LTOT_{100}, respectively. The atmospheric parameters can then be derived from the following equations:

$$L_0 = \mathrm{LTOT}_0 \tag{3}$$

$$S = \frac{\Delta_{100} - 2 \times \Delta_{50}}{\Delta_{100} - \Delta_{50}} \tag{4}$$

where $\Delta_{100} = \mathrm{LTOT}_{100} - \mathrm{LTOT}_0$ and $\Delta_{50} = \mathrm{LTOT}_{50} - \mathrm{LTOT}_0$;

$$G = \Delta_{100} \times (1 - S). \tag{5}$$

The parameters L_0, S, and G are spectral variables and dependent on atmospheric conditions such as visibility and aerosol types. In the absence of in situ measured atmospheric composition data and meteorological data over the study area at the moment of the satellite overpass, these parameters can be simulated for various atmospheric conditions and viewing geometries so as to form LUTs.

The generated LUTs included atmospheric visibilities of 5, 10, 20, and 40 km. The atmospheric model used for the simulations was mid-latitude summer, and the candidate aerosol types were maritime, rural, desert, urban, tropical, and Navy maritime with air mass character of 3 (default value). The zenith angles of sun and viewing were respectively varied from 0° to 70° (5° interval), and the relative viewing azimuth varied over the angles of 0°, 45°, 90°, 135°, and 180°. Atmospheric components such as CO_2, water vapor, and ozone gas were set to 380 ppmv, 4.0 g/cm^2, and 0.27 atm-cm, respectively.

The created LUTs are then applied to solve the inverse problem. The retrieval of reflectance (radiance) at the bottom of the atmosphere from TOA radiance was based on constants of L_0, S, and G simulated for various situations:

$$r = \frac{L^{\mathrm{TOA}} - L_0}{G + (L^{\mathrm{TOA}} - L_0)S} \tag{6}$$

For a Lambertian surface, the relationship between the directional surface radiance L and the total incident irradiance E_i is given by $L = rE_i/\pi$, while the remote-sensing reflectance is defined by $R_{rs} = L/E_i$, which thus implies that $R_{rs} = r/\pi$.

References

Berk, A., G.P. Anderson, P.K. Acharya, J.H. Chetwynd, L.S. Bernstein, E.P. Shettle, et al. 2000. MODTRAN4 users manual. Air Force Research Laboratory, Space Vehicles Directorate, Air Force Materiel Command, Hanscom AFB, MA 01731–3010, USA, p. 97.

Bézy, J.-L., S. Delwart, and M. Rast. 2002. MERIS—A new generation of ocean-colour sensor onboard Envisat. *ESA Bulletin Number 103*, August 2000. http://envisat.esa.int/news/meris103.pdf.

Carder, K.L., P.H. Reinersman, R.F. Chen, and F. Muller-Karger. 1993. AVIRIS calibration and application in coastal oceanic environments. *Remote Sensing of Environment* 44: 205–216.

Chen, S.L., G.A. Zhang, and S.L. Yang. 2003. Temporal and spatial changes of suspended sediment concentration and resuspension in the Yangtze River estuary. *Journal of Geographical Sciences* 13(4): 498–506.

Claustre, H., and S. Maritorena. 2003. The many shades of ocean blue. *Science* 302: 1514–1515.

Dasgupta, S., R.P. Singh, and M. Kafatos. 2009. Comparison of global chlorophyll concentrations using MODIS data. *Advances in Space Research* 43: 1090–1100.

Doerffer, R., and H. Schiller. 2007. The MERIS case 2 water algorithm. *International Journal of Remote Sensing* 28: 517–535.

Doerffer, R. and H. Schiller. 2008. MERIS Regional coastal and lake case 2 water project—atmospheric correction ATBD, GKSS research center 21502 Geesthacht, version 1.0 18. May 2008.

Doxaran, D., J.M. Froidefond, S. Lavender, and P. Castaing. 2002. Spectral signature of highly turbid waters: application with SPOT data to quantify suspended particulate matter concentrations. *Remote Sensing of Environment* 81: 149–161.

Doxaran, D., J.M. Froidefond, P. Castaing, and M. Babin. 2009. Dynamics of the turbidity maximum zone in a macrotidal estuary (the Gironde, France): Observations from field and MODIS satellite data. *Estuarine, Coastal and Shelf Science* 81: 321–332.

Fargion, G.S., and J.L. Muller. 2000. Ocean optics protocols for satellite ocean color sensor validation, revision 2. NASA TM-2000-209966, GSFC. Available at: http://seabass.gsfc.nasa.gov/docs/SIMBIOS-OOPR2.pdf.

Fettweis, M., B. Nechad, and D. Van den Eynde. 2007. An estimate of the suspended particulate matter (SPM) transport in the southern North Sea using SeaWiFS images, *in situ* measurements and numerical model results. *Continental Shelf Research* 27: 1568–1583.

Gordon, H.R., O.B. Brown, and M.M. Jacobs. 1975. Computed relationships between the inherent and apparent optical properties of a flat, homogeneous ocean. *Applied Optics* 14: 417–427.

Gordon, H.R., and M. Wang. 1994. Retrieval of water-leaving radiance and aerosol optical thickness over the oceans with SeaWiFS: A preliminary algorithm. *Applied Optics* 33: 443–452.

He, Q., C.X. Yun, and F.R. Shi. 1999. Remote sensing analysis for suspended sediment concentration in water surface layer in Yangtze River estuary. *Progress in Natural Science (in Chinese with an English abstract)* 9: 160–164.

Hu, C., Z.Q. Chen, T.D. Clayton, P. Swarzenski, J.C. Brock, and F.E. Muller-Karger. 2004. Assessment of estuarine water-quality indicators using MODIS medium-resolution bands: Initial results from Tampa Bay, FL. *Remote Sensing of Environment* 93: 423–441.

IOCCG. 2000. Remote sensing of ocean color in coastal, and other optically-complex, waters. In Reports of the International Ocean-Color Coordinating Group, No. 3, ed. Sathyendranath, S. IOCCG, Dartmouth, Canada.

Lee, Z.P., K.L. Carder, T.G. Peacock, C.O. Davis, and J.L. Mueller. 1996. Method to derive ocean absorption coefficients from remote-sensing reflectance. *Applied Optics* 35: 453–462.

Lee, Z.P., and C. Hu. 2006. Global distribution of case-1 waters: An analysis from SeaWiFS measurements. *Remote Sensing of Environment* 101: 270–276.

Li, J.F., W.R. Shi, and H.T. Shen. 1994. Sediment properties and transportation in the turbidity maximum in Changjiang estuary. *Geographical Research* 13: 51–59 (in Chinese with an English abstract).

Krivtsov, V., M.J. Howarth, and S.E. Jones. 2009. Characterising observed patterns of suspended particulate matter and relationships with oceanographic and meteorological variables: Studies in Liverpool Bay. *Environmental Modelling & Software* 24: 677–685.

Kong, Y.Z., P.X. Ding, S.L. He, C. He, and W.J. Xiao. 2006. Analysis of spatial and temporal variation characteristics of suspended sediment concentration in the Changjiang River Estuary and adjacent sea area. *Advances in Marine Science* 24: 446–454 (in Chinese with an English abstract).

Kubelka, P., and F. Munk. 1931. Ein beitrag zur optik der farbanstriche. *Z Techn Physik* 12: 593–601.

Miller, R.L., and B.A. McKee. 2004. Using MODIS Terra 250 m imagery to map concentrations suspended matter in coastal waters. *Remote Sensing of Environment* 93: 259–266.

Mobley, C.D. 1999. Estimation of the remote-sensing reflectance from above-surface measurements. *Applied Optics* 38: 7442–7455.

Schroeder, Th, I. Behnert, M. Schaale, J. Fischer, and R. Doerffer. 2007. Atmospheric correction algorithm for MERIS above case-2 waters. *International Journal of Remote Sensing* 28(7): 1469–1486.

Shen, H.T., and D. Pan. 2001. *Turbidity maximum in the Changjiang estuary*, 194. Beijing: China Ocean Press (in Chinese).

Shen, F., M.S. Salama, Y.X. Zhou, J.F. Li, Z. Su, and D.B. Kuang. 2010. Remote-sensing reflectance characteristics of highly turbid estuarine waters—A comparative experiment of the Yangtze River and the Yellow River. *International Journal of Remote Sensing* 31(10): 2639–2654.

Shen, F., and W. Verhoef. 2010. Suppression of local haze variations in MERIS images over turbid coastal waters for retrieval of suspended sediment concentration. *Optics Express* 18(12): 12653–12662. doi:10.1364/OE.18.012653.

Verhoef, W., and H. Bach. 2003. Simulation of hyperspectral and directional radiance images using coupled biophysical and atmospheric RT-models. *Remote Sensing of Environment* 87: 23–41.

Yang, S.L., J. Zhang, and X.J. Xu. 2007. Influence of the Three Gorges Dam on downstream delivery of sediment and its environmental implications, Yangtze River. *Geophysical Research Letters* 34: L10401. doi:10.1029/2007GL029472.

Zhang, J., Y. Wu, T.C. Jennerjahn, V. Ittekkot, and Q. He. 2007. Distribution of organic matter in the Changjiang (Yangtze River) Estuary and their stable carbon and nitrogen isotopic ratios: Implications for source discrimination and sedimentary dynamics. *Marine Chemistry* 106(1–2): 111–126.